AIAA JOURNAL
Vol. 30, No. 5, May 1992

Compressible Turbulent Boundary Layers with Heat Addition by Homogeneous Condensation

Günter H. Schnerr* and Rainer Bohning†
University (TH) of Karlsruhe, D-W-7500, Karlsruhe 1, Germany
Thomas Breitling‡
Daimler-Benz AG, D-W-7000 Stuttgart 80, Germany
and
Hans-Arno Jantzen§
University (TH) of Karlsruhe, D-W-7500, Karlsruhe 1, Germany

Homogeneous condensation in transonic viscous flow is computed using a combination of analytical and numerical methods. The procedure is based on the perturbance method for the shock/boundary-layer interaction of Bohning and Zierep for adiabatic flow. In this paper, the model was extended for applications to boundary-layer flows with internal nonequilibrium heat addition. For the simulation of the homogeneous condensation process we use the classical nucleation theory of Volmer and the molecular Hertz-Knudsen droplet growth law. One momentum equation of the Navier-Stokes equations is solved by a time-stepping procedure combined with a mixing length turbulence model. Objective in view is the analysis of the macroscopic phenomena of non-equilibrium heat addition from homogeneous condensation of water vapor in transonic flows with high velocity and temperature gradients normal to the main flow direction. In detail, the cooling rate, the nucleation rate, the droplet radius, and the condensate mass fraction in the boundary layer are discussed. Approaching the wall surface and in comparison to the inviscid diabatic flow just outside of the boundary layer the nucleation process and the deposition of droplets, i.e. the condensate fraction contours, are shifted downstream, continuously or stepwise, depending on the pressure gradients at the boundary-layer edge. From the comparison of the integral boundary layer variables we conclude that the friction coefficients change only moderately, whereas the displacement and momentum thickness are found to be more sensitive to the homogeneous condensation onset.

Nomenclature

c_p = specific heat at constant pressure
g = condensate mass fraction
J = nucleation rate
m = mass per molecule
M = Mach number
p = pressure
$p_{s,r}$ = saturation pressure of droplet with radius r
Q = rate of heat addition
q = normalized rate of heat addition
r = droplet radius
$\bar{r}$ = surface averaged droplet radius
R = specific gas constant, radius of wall curvature
S = saturation ratio
T = absolute temperature
u = tangential velocity
v = normal velocity
x = Cartesian coordinate, mixing ratio
y = Cartesian coordinate
α = condensation coefficient
β = shape factor
γ = specific heat ratio
ϕ = relative humidity
ρ = density
σ = surface tension

Subscripts and Superscripts

B = basic values
c = condensate, condensation onset
d = disturbance values
f = frozen
s = saturation
v = vapor
δ = values at the boundary layer edge
0 = stagnation condition, inflow boundary
1 = before heat addition
∞ = plane surface
$*$ = critical values at $M = 1$

Received Sept. 4, 1990; revision received June 21, 1991; accepted for publication July 17, 1991.

*Privatdozent (Fluid Dynamics), Dr.-Ing. habil., Institut für Strömungslehre und Strömungsmaschinen, Department of Mechanical Engineering, Kaiserstrasse 12. Senior Member AIAA.

†Prof. Dr.-Ing. habil., Institut für Strömungslehre and Strömungsmaschinen, Department of Mechanical Engineering, Kaiserstrasse 12.

‡Dr.-Ing., Direktion Technik, P.O. Box 800260.

§Dr.-Ing, Institut für Strömungslehre and Strömungsmaschinen, Department of Mechanical Engineering, Kaiserstrasse 12.

Introduction

CONDENSATION phenomena in transonic flow are relevant for numerous technical and scientific applications. In steam turbines the development of droplets must be controlled because of erosion effects. In cryogenic wind tunnels and shock tubes the homogeneous condensation onset of pure nitrogen has to be avoided. Other applications can be found in chemical reactions and in rocket engines.

Transonic experiments with moist air show stationary condensation processes for supply conditions of relative humidities up to about 75%. Condensation onset and structure of the heat addition zone in the inviscid region just outside of the boundary layer depend on the relative and absolute humidity, the geometry of the problem, and on boundary-layer effects. In transonic Laval nozzle and airfoil flows the onset

of heat addition penetrates the boundary layer. As the interference area we define a region of the thickness δ_0 (thickness of the oncoming boundary layer) beginning near the nozzle throat far upstream of the nucleation onset and ending behind the sudden nonequilibrium heat release, where a weak equilibrium condensation process prevails. Inside of this interference area the calculation includes both, the pressure gradients and the heat addition.

Simplified models for viscous flows with homogeneous condensation and evaporation were investigated in Studzinsky[1] and Ryley[2]. Visualization by light scattering of transonic condensing flow over airfoils shows clearly the existence of a near wall zone without droplets[3]. In the present work, a new and more accurate procedure for the calculation of the condensation process in transonic turbulent boundary layers is developed. For the first time analytical and numerical methods are used to combine the classical nucleation theory and the Hertz-Knudsen growth law with a compressible boundary-layer algorithm. Our model leads to the understanding of the interaction of homogeneous nucleation and viscosity effects and allows the appreciation of their influence on the integral boundary layer quantities, e.g., displacement and momentum thickness, and on the friction coefficient.

Method of Calculation

Our method is based on the analytical perturbation theory of Bohning[4] and Bohning and Zierep[5] and Oswatitsch and Zierep.[7] The original model computes the shock/boundary-layer interaction in purely adiabatic flow and for adiabatic wall conditions. This analytical model is modified and combined with two numerical methods. On the one hand, the momentum equation in flow direction is solved by a time-stepping procedure to compute the tangential component of the velocity. This calculation removes the asymptotic character of the purely analytical solution and includes a more accurate description of the flow in extended interference areas. On the other hand, a procedure was developed to include the classical nucleation theory of Volmer and the molecular Hertz-Knudsen droplet growth law for description of the homogeneous condensation process.

Analytical Part

The perturbance theory is based on Lighthill's theory.[8] He found that for the computation of disturbances in a compressible shear layer, the viscous terms of the Navier-Stokes equations play a minor role. To render the boundary layer accessible to an analytical treatment, it is subdivided into a shear layer and a sublayer close to the wall, where viscous effects are fully active. Then the disturbance equations can be solved analytically by a separation method.

In perturbation form, the equations for the continuity of mass, momentum, and energy and the equation of state become

$$\rho_B \frac{\partial u_d}{\partial x} + \frac{\partial \rho_B v_d}{\partial y} + M_B^* \frac{\partial \rho_d}{\partial x} = 0 \tag{1}$$

$$\rho_B M_B^* \frac{\partial u_d}{\partial x} + \rho_B v_d \frac{\mathrm{d}M_B^*}{\mathrm{d}y} = -\frac{1}{\gamma} \frac{\partial p_d}{\partial x} \tag{2}$$

$$\rho_B M_B^* \frac{\partial v_d}{\partial x} = -\frac{1}{\gamma} \frac{\partial p_d}{\partial y} \tag{3}$$

$$T_d + M_B^* u_d(\gamma - 1) = q \tag{4}$$

$$\rho_B T_d + \rho_d T_B = p_d \tag{5}$$

All variables are reduced by the critical values of the inviscid flow. The heat addition is normalized by $q = Q/(c_p T^*)$. The boundary conditions required for the disturbance computation are: 1) velocity profile at the inflow area, approximated by $u/u_\delta = (y/\delta)\beta$; 2) constant pressure normal to the main flow direction at the inflow and the outflow boundary of the interference area; 3) static pressure distribution and temperature at the boundary-layer edge, given from the inviscid calculation of the outer flowfield; and 4) no-slip condition at the wall. First, the system of the Eqs. (1–5) is reduced into one equation. With the boundary conditions from above, this equation can be solved analytically using Fourier's separation method. The main contents of this method is an eigenvalue problem normal to the wall, which is solved in a closed form by hypergeometric series.

With this method, the insensitive quantities pressure p, density ρ, and normal velocity v are obtained in a high accuracy. The tangential velocity u is more sensitive even near the wall in the limit to separation onset. In this case the disturbance model is no longer valid. Therefore, the tangential velocity is calculated by the first Navier-Stokes equation in x direction introducing a suitable turbulence model. A more detailed description of the analytical work can be found in Refs. 4–6.

Numerical Calculation of the Momentum Equation

The momentum equation is solved by a finite difference scheme following Beam and Warming.[9] An implicit algorithm is used to find the steady solution. Density, static pressure, and the normal velocity are given as coefficients from the analytical solution. As the additional boundary condition solving the Navier-Stokes equation we use $u_{xx} = 0$ at the outflow boundary. The sensitivity of the numerical solution to this boundary condition has been checked by variation of the length of the interference area up to 400%. At a fixed reference point downstream of the main pressure variations, the changements of displacement and momentum thickness were less than 2%.

We have implemented a two-layer turbulence model after Cebeci and Smith.[10] The needed damping factor for the inner layer is dependent on the pressure gradient, according to experimental investigations. The damping factor and pressure gradient are correlated following the formulation of Refs. 11 and 12. The combination of the analytical solution and the numerical method of the momentum equation is proven by preceeding investigations of adiabatic shock/boundary-layer interferences.[12,13] An extension of the local solution method to finite traversed distance has been made. Long distances computed with this model require a correction of the normal velocity distribution. It was determined by comparison with experiments in Ref. 12.

Calculation of the Homogeneous Condensation

On the basis of the classical nucleation theory[14] the rate of heat addition is computed along different streamlines in the boundary layer. The nucleation rate J per unit time and volume is given by

$$J = \sqrt{\frac{2}{\pi}} \sqrt{\sigma_\infty} m^{-1.5} \frac{\rho_v^2}{\rho_c} \exp\left(-\frac{16}{3} \pi \frac{\sigma_\infty^3}{m \rho_c^2 R_v^3 T^3 \mathscr{A}^2(\mathrm{S})} \right) \tag{6}$$

The surface tension is dependent on the temperature. For liquid condensate we use the empirical relationship of Schnerr and Dohrmann.[15] Along all streamlines the surface averaged droplet radius $\bar{r}$[16] is smaller than the mean free path of the molecules λ. Consequently the droplet growth is calculated following the molecular Hertz-Knudsen growth law, i.e., the temperature of the droplet and the surrounding vapor are assumed to be equal. The condensation coefficient α is set to unity. For the condensate mass fraction g we have

$$\frac{\mathrm{d}g}{\mathrm{d}t} = \frac{4}{3} \pi \rho_c \frac{J}{\rho} + \int_{-\infty}^{t} \frac{4}{3} \pi \rho_c \frac{J(t_1)}{\rho(t_1)} \frac{\mathrm{d}r^3(t_1)}{\mathrm{d}t} \mathrm{d}t_1 \tag{7}$$

$$\frac{dr}{dt} = \frac{\alpha}{\rho_c}\frac{p_v - p_{s,r}}{\sqrt{2\pi R_v T}} \tag{8}$$

which can be transformed into a system of four coupled differential equations.[16]

Operating Sequence of the Total Procedure

The iteration sequence is controlled so that after every analytical calculation step a certain number of iterations of the momentum equation follows. Changed velocity distributions give the new boundary condition for a further calculation of the homogeneous condensation. An updated heat addition is prescribed in the next iteration step. The computation is finished when the maximum correction of the heat addition values per iteration is lower than a provided threshold limit. A stationary solution was reached in general in about 4 min on an IBM 3090.

Results

Two different boundary layer regions in a plane Laval nozzle flow with different pressure gradients are analyzed: 1) the boundary-layer region at the nozzle wall; and 2) the boundary-layer region at the side wall along the nozzle axis.

The pressure distributions at the boundary-layer edge are taken from diabatic, inviscid calculations performed by Dohrmann[17] and Schnerr[18] using a two-dimensional Euler solver (FVM). Figure 1 shows the numerical result of the plane Laval nozzle flow calculation. The hyperbolic nozzle has a total throat height of 2 y^* = 120 mm, a radius of curvature at the throat of 200 mm, the width is 50 mm. The Reynolds number Re_δ of the boundary layer at the inflow of the inter-

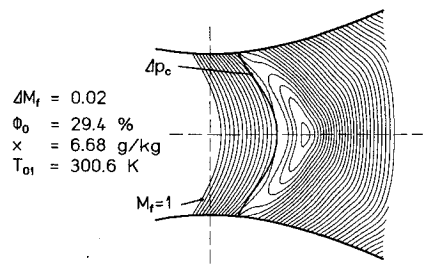

Fig. 1 Heat addition caused by homogeneous condensation of water vapor in moist air in a hyperbolic Laval nozzle, 2 y^* = 120 mm, R^* = 200 mm, temperature gradient $(dT/dx)^*$ = −5.1°C/cm (theory), flow from left. Plotted are frozen iso-Mach lines $M_f \geq 1$, a compression of Δp_c = 2 Torr is defined as the condensation onset. x: mixing ratio $g_{H_2O}/kg_{dry\ air}$.

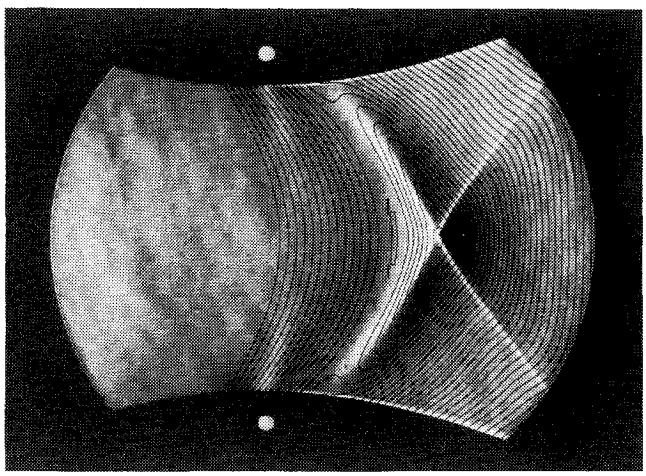

Fig. 2 Schlieren picture with "Condensation X-shock," ϕ_0 = 29.2%, mixing ratio x = 6.2 $g_{H_2O}/kg_{dry\ air}$, T_{01} = 299.4 K, flow from left, iso-Mach lines $M_f \geq 1$, increment ΔM_f = 0.02.

ference area is 21,000. Figure 2 shows a schlieren picture of a "Condensation X-shock" and the comparison with calculated iso-Mach lines beginning at the sonic line. The bright parabolic area corresponds to the continuous supersonic compression from the heat addition which creates the characteristic oblique shocks. Due to the higher gradients in main flow direction the diabatic effects weaken towards the nozzle walls.

Interference Area at the Nozzle Wall

First we discuss the region at the nozzle wall. Figure 3 shows the diabatic and the adiabatic Mach number distribution at the boundary-layer edge with the characteristic weak supersonic compression for low rates of heat addition. Adiabatic temperature contours in the boundary layer are shown in Fig.4. δ_0 is the boundary-layer thickness at the inflow boundary. Generally, x = 0 corresponds to the nozzle throat position. The nearly horizontal lines represent three streamlines. At a fixed location x = const the temperature rises approaching the wall. Consequently the supersaturation decreases and the process of nucleation and droplet growth is weakened and vanishes very near the wall. Figure 5 shows the temperature contours of the diabatic flowfield. Compared with the adiabatic flow the temperature increases locally. This results from the latent heat release inside and outside of the boundary

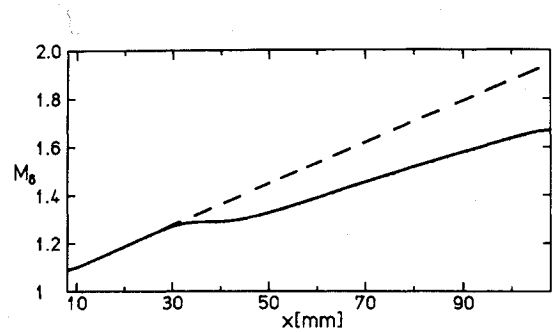

Fig. 3 Adiabatic (– – –) and diabatic (——) Mach number along the boundary-layer edge-nozzle wall.

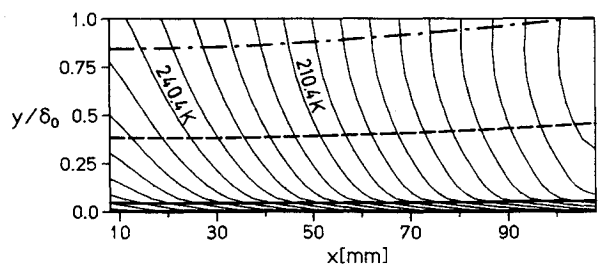

Fig. 4 Temperature contours in the boundary layer, contour increment ΔT = 6 K, adiabatic flow—nozzle wall. The three nearly horizontal lines represent streamlines. δ_0 is the boundary-layer thickness at the inflow boundary.

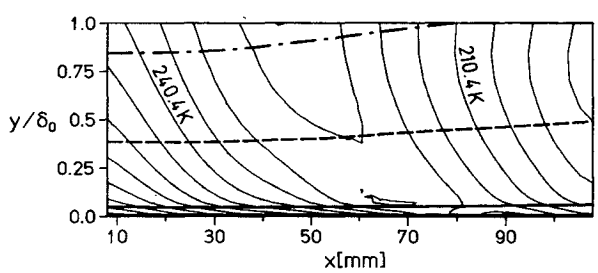

Fig. 5 Temperature contours in the boundary layer, contour increment ΔT = 6 K, diabatic flow-nozzle wall. The three nearly horizontal lines represent streamlines.

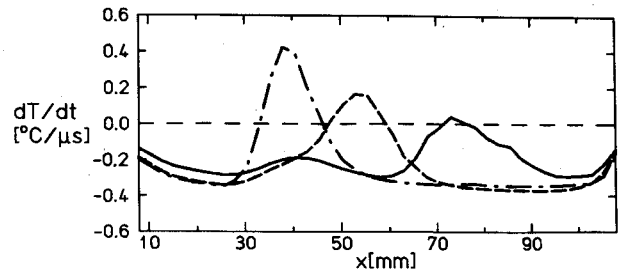

Fig. 6 Cooling rate along streamlines in the boundary layer, diabatic flow-nozzle wall: (— · — · —) outer streamline; (– – –) middle streamline; (——) inner streamline.

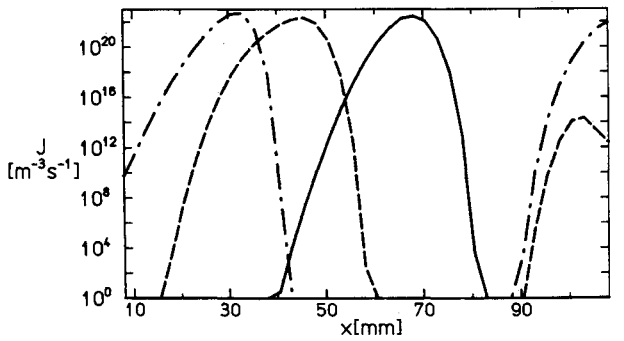

Fig. 7 Homogeneous nucleation rate along streamlines in the boundary layer-nozzle wall: (— · — · —) outer streamline; (– – –) middle streamline; (——) inner streamline.

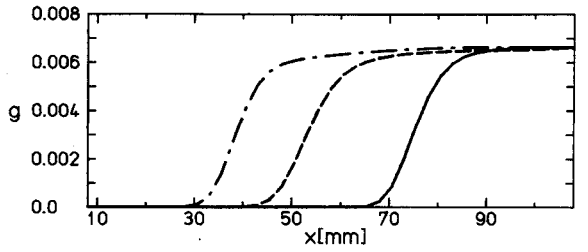

Fig. 8 Development of the condensate mass fraction along streamlines in the boundary layer-nozzle wall: (— · — · —) outer streamline; (– – –) middle streamline; (——) inner streamline.

layer. From experiments as well as from inviscid calculations the dominating influence of the cooling rate (dT/dt) [°C/μs] on the condensation onset is known. The analytical expression for this parameter for inviscid nozzle flows is given from Wegener[19] and Wegener and Mack[20]. As a first result, the diabatic cooling rates along the plotted streamlines are shown in Fig. 6. Approaching the wall the maximum decreases and is shifted downstream. Simultaneously the maximum of the nucleation rate (Fig. 7) moves downstream to different locations. It is located in the region of the lowest local temperature when the cooling rate is equal to zero. In zones of lower temperatures the nucleation process recommences. The droplet growth depends on the temperature and on the difference between surrounding vapor pressure and saturation pressure at the droplet surface. From the characteristics of the nucleation rates we expect a similar structure for the condensate mass fraction distributions along the three streamlines, which are shown in Fig. 8. The onset moves downstream for higher temperatures near the wall and rises to the same maximum level (constant supply conditions). Condensate mass fraction contours in the whole boundary layer are shown in Fig. 9. The condensation onset is defined at a condensate mass fraction of $g_c = 0.1\ g_{H_2O}/kg_{mixture}$. Figure 10 shows the surface averaged droplet radius along the discussed streamlines. Comparing the nucleation process (Fig. 7) and the development of the condensate mass fraction (Fig. 8) for the different streamlines it can be seen that at the upper and the lower one the nucleation rate and the condensate mass fraction grow a little bit faster and the absolute number of nuclei becomes higher. As a result, the surface-averaged droplet radii are smaller at the streamline than in the middle. The dip at the lower line is a characteristic nonphysical effect using Hill's surface-averaged droplet radius model and has no influence on the results in the condensing area.

In Fig. 11 we compare the compressible displacement and momentum thickness with the corresponding values of the adiabatic flow (dashed). The decrease of the displacement thickness and the increase of the momentum thickness at the

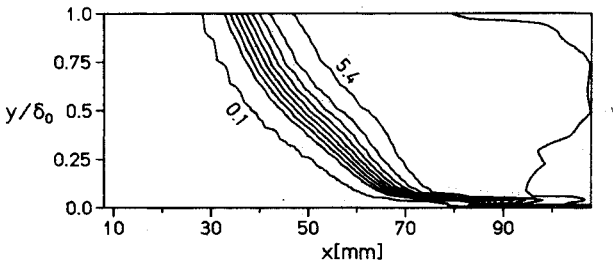

Fig. 9 Condensate mass fraction contours g [$g_{H_2O}/kg_{mixture}$] in the boundary layer-nozzle wall, contour increment $\Delta g = 0.6\ g_{H_2O}/kg_{mixture}$, $g = 0.1\ g_{H_2O}/kg_{mixture}$ corresponds to the condensation onset.

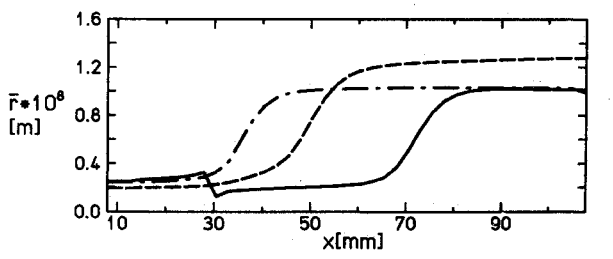

Fig. 10 Surface averaged droplet radius $\bar{r}$ along streamlines in the boundary layer-nozzle wall: (— · — · —) outer streamline; (– – –) middle streamline; (——) inner streamline.

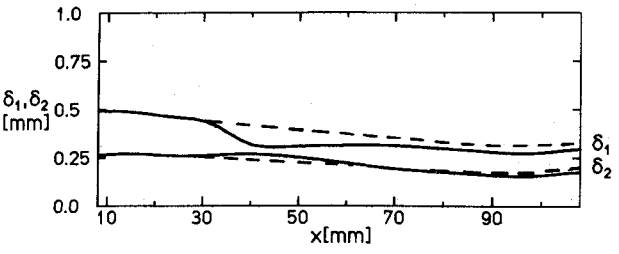

Fig. 11 Comparison between adiabatic (– – –) and diabatic (——) displacement (δ_1) and momentum (δ_2) thickness-nozzle wall.

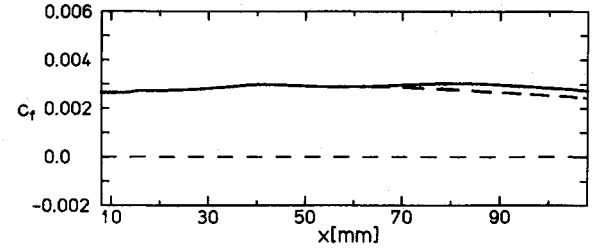

Fig. 12 Development of the adiabatic (– – –) and diabatic (——) friction coefficient-nozzle wall.

condensation onset in the outer layers are typical. This decrease of the displacement thickness occurs in spite of the lower acceleration and can be explained by the density variation. At the right-hand side of the interference area, both the displacement and the momentum thickness are reduced in comparison to the adiabatic flow and the friction coefficient becomes higher (Fig. 12). In the case of heat addition from homogeneous condensation, the friction coefficient remains nearly unchanged in the area of the condensation onset.

Interference Area at the Sidewall-Nozzle Axis

In our second example we reduce the pressure gradient in main flow direction of the inviscid flow. This condition represents the flow along the sidewall at the nozzle axis (dashed horizontal line in Fig. 1). The reduced adiabatic Mach number gradient at the boundary-layer edge is shown in Fig. 13. Nevertheless, the condensate mass fraction rises to the same maximum amount. In the diabatic case, the heat addition in the outer flowfield causes a well-marked deceleration. This stronger compression results in a different behavior of the condensation process compared with the first example, i.e. the relative influence of the same maximum heat addition is strengthened. Figure 14 shows the diabatic temperature contours. Again, three streamlines are discussed with the same

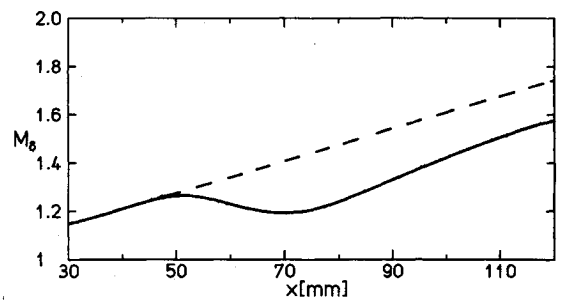

Fig. 13 Adiabatic (– – –) and diabatic (——) Mach number along the boundary-layer edge, sidewall-nozzle axis.

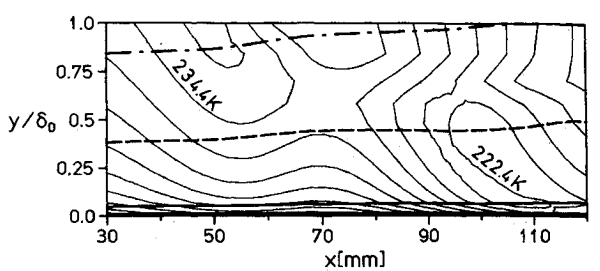

Fig. 14 Diabatic temperature contours and streamlines in the sidewall boundary layer-nozzle axis, contour increment ΔT = 6 K.

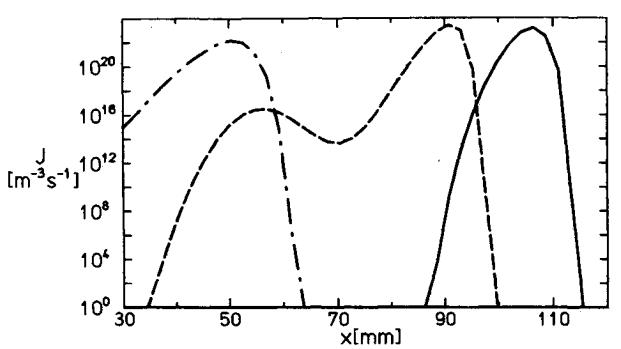

Fig. 15 Homogeneous nucleation rate along streamlines, sidewall boundary layer-nozzle axis: (— · — · —) outer streamline; (– – –) middle streamline; (——) inner streamline.

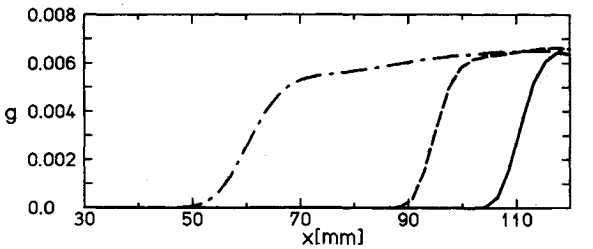

Fig. 16 Development of the condensate mass fraction along streamlines, sidewall boundary layer-nozzle axis: (— · — · —) outer streamline; (– – –) middle streamline; (——) inner streamline.

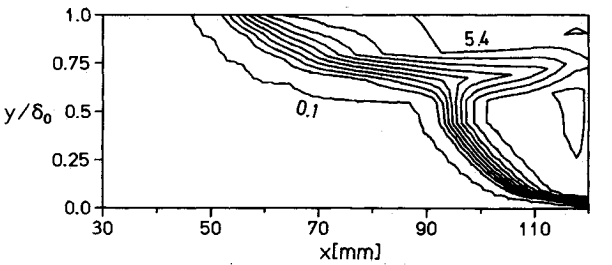

Fig. 17 Condensate mass fraction contours in the boundary layer-nozzle axis, contour increment $\Delta g = 0.6\, g_{H_2O}/kg_{mixture}$.

coordinates at the inflow boundary as before. Figures 15 and 16 show the nucleation rate and the condensate mass fraction. Along the outer streamline (represented by the dashed/dotted line) the processes of nucleation and droplet growth are nearly identical to those in the outer flowfield. There is only a minimal effect of weakening and shifting downstream. In addition to the heat, produced by friction effects, the change of the thermal conditions is well marked. The maximum nucleation rate, relevant to the condensation onset, obviously is shifted further downstream with the consequence of an additional delay of the nucleation process close to the wall. In conclusion, the condensation onset near the wall is delayed by the latent heat release in outer layers (Fig. 17).

Conclusion

A combination procedure consisting of analytical and numerical methods simulates transonic boundary-layer flow with nonequilibrium heat addition by homogeneous condensation. The development of the perturbation theory of Bohning and Zierep[5,6] was extended. Our method calculates the interference region near the onset of nucleation and heat addition close to the wall.

In this flow with high gradients of temperature and velocity normal to the flow direction, the heating front moves downstream with decreasing distance to the wall. The interference of compression zones caused by heat addition in the outer flowfield leads to different shapes of the heating front in the boundary layer dependent on the pressure gradient in main flow direction of the adiabatic reference case. The first example with the higher gradient has been located at the nozzle wall. The second example (lower gradient, sidewall area) leads to the same maximum amount of heat addition. Here, a stepwise shifted condensate onset occurs with varying distance to the wall. These effects have been explained using temperature contours, regarding the cooling rate, the nucleation rate, and the droplet growth on different streamlines. The resulting condensate mass fraction contours demonstrate the interference of adjacent layers. Heat addition from homogeneous condensation inside a boundary layer may lead to a relative or absolute increase of the friction coefficient, e.g. at the end of the interference area at the nozzle wall the friction coefficient is about 8% higher than without homogeneous con-

densation. Simultaneously, the displacement and momentum thickness decrease 12% and 15%, respectively. The comparison of integral boundary layer quantities with the corresponding values in the adiabatic flow allows the appreciation of the reaction on the inviscid flow.

Acknowledgment

This work was partially supported by the Deutsche Forschungsgemeinschaft (DFG-contract Zi-18/32) and the Volkswagenstiftung.

References

[1]Studzinsky, W., "Boundary Layer in Compressible Flow of Wet Water Vapour," *International Journal of Multiphase Flow*, Vol. 5, No. 3, 1979, pp. 185–199.

[2]Ryley, D. J., "The Behaviour of Nucleation Fogs within the Nozzle Boundary Layers in the Wet Steam Turbine," *Journal of Mechanical Engineering Science*, Vol. 13, No. 3, 1971, pp. 190–199.

[3]Hiller, W. J., Meier, G. E. A., "Experimentelle Untersuchung einer transsonischen Potentialströmung um ein symmetrisches Tragflügelprofil," Max Planck-Institut für Strömungsforschung, Bericht 10, Göttingen, Germany, 1971.

[4]Bohning, R., "Die Wechselwirkung eines senkrechten Verdichtungsstoßes mit einer turbulenten Grenzschicht an einer gekrümmten Wand," Habilitationsschrift, Universität (TH) Karlsruhe, Karlsruhe, Germany, 1982.

[5]Bohning, R., and Zierep, J., "Der senkrechte Verdichtungsstoß an der gekrümmten Wand unter Berücksichtigung der Reibung," *Zeitschrift für Angewandte Mathematik und Physik (ZAMP)*, Vol. 27, No. 2, 1976, pp. 225–240.

[6]Bohning, R., and Zierep, J., "Normal Shock-Turbulent Boundary Layer Interaction at a Curved Wall," Computation of Viscous-Inviscid Interactions, AGARD CP 291, 1980, pp. 17.1–17.8.

[7]Oswatitsch, K., and Zierep, J., "Das Problem des senkrechten Stoßes an einer gekrümmten Wand," *Zeitschrift für Angewandte Mathematik und Mechanik (ZAMM)*, Vol. 40, 1960, pp. 143–144.

[8]Lighthill, M. J., "Interactions between Normal Shock Waves and Turbulent Boundary Layers," Ames Research Center (NASA); British Aeronautical Research Council, R&M 3262, 1961.

[9]Beam, R. M., Warming, R. F., "An Implicit Factored Scheme for the Compressible Navier-Stokes Equations," *AIAA Journal*, Vol. 16, No. 4, 1978, pp. 393–402.

[10]Cebeci, T., Smith, A. M. O., "Analysis of Turbulent Boundary Layers," *Applied Mathematics and Mechanics*, edited by F. N. Frenkiel and G. Temple, International Series of Monographs, Academic Press, New York 1974.

[11]Chen, C. L., "Computation of Transonic Flow over Porous Airfoils," Ph.D. Dissertation, University of Colorado, Boulder, CO, 1986.

[12]Breitling, T., "Berechnung transsonischer, reibungsbehafteter Kanal und Profilströmungen mit passiver Beeinflussung," Ph.D. Dissertation, Universität (TH) Karlsruhe, Karlsruhe, Germany, 1989.

[13]Bohning, R., Jungbluth, H., "Turbulent Shock/Boundary Layer Interaction with Control," *Symposium Transsonicum III*, edited by J. Zierep and H. Oertel, Springer-Verlag, Berlin, 1989, pp. 389–398.

[14]Volmer, M., *Kinetik der Phasenbildung*, Steinkopf, Leipzig, Germany, 1939.

[15]Schnerr, G. H., and Dohrmann, U., "Transonic Flow Around Airfoils with Relaxation and Energy Supply by Homogeneous Condensation," *AIAA Journal*, Vol. 28, No. 7, 1990, pp. 1187–1193. See also: AIAA Paper 89-1834, Twentieth Fluid Dynamics, Plasma Dynamics, and Lasers Conference, Buffalo, NY, June 1989.

[16]Hill, P. G., "Condensation of Water Vapor During Supersonic Expansion in Nozzles," *Journal of Fluid Mechanics*, Vol. 25, Part 3, 1966, pp. 593–620.

[17]Dohrmann, U., "Ein numerisches Verfahren zur Berechnung stationärer transsonischer Strömungen mit Energiezufuhr durch homogene Kondensation," Ph.D. Dissertation, Universität (TH) Karlsruhe, Germany, 1989.

[18]Schnerr, G. H., and Dohrmann, U., "Ein numerisches Verfahren zur Berechnung stationärer transsonischer Strömungen mit Relaxation und Wärmezufuhr, *Zeitschrift für Angewandte Mathematik und Mechanic (ZAMM)*, Vol. 69, No. 6, 1989, pp. 588–591.

[19]Wegener, P. P., "Condensation Phenomena in Nozzles," *Progress in Astronomy and Aeronautics*, Vol. 15, Academic Press, New York, 1964, pp. 701–742.

[20]Wegener, P. P., and Mack, L. M., "Condensation in Supersonic and Hypersonic Wind Tunnels," *Advances in Applied Mechanics 5*, edited by H. L. Dryden and T. Kàrmàn, Academic Press, New York, 1958, pp. 307–477.